Annals of Nuclear Energy 227 (2026) 111977

Contents lists available at ScienceDirect

Annals of Nuclear Energy

journal homepage: www.elsevier.com/locate/anucene

Measurement of the ^{244}Cm neutron capture cross section at the n_TOF facility at CERN

V. Alcayne [1,*], A. Kimura [2], E. Mendoza [1], D. Cano-Ott [1], O. Aberle [3], F. Álvarez-Velarde [1], S. Amaducci [4,5], J. Andrzejewski [6], L. Audouin [7], V. Babiano-Suarez [8], M. Bacak [3,9,10], M. Barbagallo [3,11], F. Bečvář [12], V. Bécares [1], G. Bellia [4,5], E. Berthoumieux [10], J. Billowes [13], D. Bosnar [14], A. Brown [15], M. Busso [16,17], M. Caamaño [18], L. Caballero-Ontanaya [8], F. Calviño [19], M. Calviani [3], A. Casanovas [19], F. Cerutti [3], Y.H. Chen [7], E. Chiaveri [3,13,20], N. Colonna [11], G. Cortés [19], M.A. Cortés-Giraldo [20], L. Cosentino [4], S. Cristallo [16,21], L.A. Damone [11,22], M. Diakaki [23,3], M. Dietz [24], C. Domingo-Pardo [8], R. Dressler [25], E. Dupont [10], I. Durán [18], Z. Eleme [26], B. Fernández-Domínguez [18], A. Ferrari [3], P. Finocchiaro [4], V. Furman [27], K. Göbel [28], R. Garg [24], A. Gawlik-Ramiega [6], S. Gilardoni [3], T. Glodariu [29], I.F. Gonçalves [30], E. González-Romero [1], C. Guerrero [20], F. Gunsing [10], H. Harada [2], S. Heinitz [25], J. Heyse [31], D.G. Jenkins [15], E. Jericha [9], F. Käppeler [32], Y. Kadi [3], N. Kivel [25], M. Kokkoris [23], Y. Kopatch [27], M. Krtička [12], D. Kurtulgil [28], I. Ladarescu [8], C. Lederer-Woods [24], H. Leeb [9], J. Lerendegui-Marco [20], S. Lo Meo [33,34], S.J. Lonsdale [24], D. Macina [3], A. Manna [34,35], T. Martínez [1], A. Masi [3], C. Massimi [34,35], P. Mastinu [36], M. Mastromarco [3], F. Matteucci [37,38], E.A. Maugeri [25], A. Mazzone [11,39], A. Mengoni [33], V. Michalopoulou [23], P.M. Milazzo [37], F. Mingrone [3], A. Musumarra [40,5], A. Negret [29], R. Nolte [41], F. Ogállar [42], A. Oprea [29], N. Patronis [26], A. Pavlik [43], A. Pérez de Rada [1], J. Perkowski [6], L. Piersanti [11,16,21], I. Porras [42], J. Praena [42], J.M. Quesada [20], D. Radeck [41], D. Ramos [7], T. Rauscher [44,45], R. Reifarth [28], D. Rochman [25], C. Rubbia [3], M. Sabaté-Gilarte [3,20], A. Saxena [46], P. Schillebeeckx [31], D. Schumann [25], A.G. Smith [13], N.V. Sosnin [13], A. Stamatopoulos [23], G. Tagliente [11], J.L. Tain [8], T. Talip [25], A. Tarifeño-Saldivia [19], L. Tassan-Got [3,23,7], P. Torres-Sánchez [42], A. Tsinganis [3], J. Ulrich [25], S. Urlass [3,47], S. Valenta [12], G. Vannini [34,35], V. Variale [11], P. Vaz [30], A. Ventura [34], V. Vlachoudis [3], R. Vlastou [23], A. Wallner [48], P.J. Woods [24], T. Wright [13], P. Žugec [14]

[1] *Centro de Investigaciones Energéticas Medioambientales y Tecnológicas (CIEMAT), Spain*
[2] *Japan Atomic Energy Agency (JAEA), Tokai-Mura, Japan*
[3] *European Organization for Nuclear Research (CERN), Switzerland*
[4] *INFN Laboratori Nazionali del Sud, Catania, Italy*
[5] *Department of Physics and Astronomy, University of Catania, Italy*
[6] *University of Lodz, Poland*
[7] *Institut de Physique Nucléaire, CNRS-IN2P3, Univ. Paris-Sud, Université Paris-Saclay, F-91406 Orsay Cedex, France*
[8] *Instituto de Física Corpuscular, CSIC - Universidad de Valencia, Spain*
[9] *TU Wien, Atominstitut, Stadionallee 2, 1020 Wien, Austria*
[10] *CEA Irfu, Université Paris-Saclay, F-91191 Gif-sur-Yvette, France*
[11] *Istituto Nazionale di Fisica Nucleare, Sezione di Bari, Italy*
[12] *Charles University, Prague, Czech Republic*
[13] *University of Manchester, United Kingdom*
[14] *Department of Physics, Faculty of Science, University of Zagreb, Zagreb, Croatia*
[15] *University of York, United Kingdom*
[16] *Istituto Nazionale di Fisica Nucleare, Sezione di Perugia, Italy*

* Corresponding author.
E-mail address: victor.alcayne@ciemat.es (V. Alcayne).

https://doi.org/10.1016/j.anucene.2025.111977
Received 26 August 2025; Received in revised form 8 October 2025; Accepted 27 October 2025
Available online 1 December 2025

[17] Dipartimento di Fisica e Geologia, Università di Perugia, Italy
[18] University of Santiago de Compostela, Spain
[19] Universitat Politècnica de Catalunya, Spain
[20] Universidad de Sevilla, Spain
[21] Istituto Nazionale di Astrofisica - Osservatorio Astronomico d'Abruzzo, Italy
[22] Dipartimento Interateneo di Fisica, Università degli Studi di Bari, Italy
[23] National Technical University of Athens, Greece
[24] School of Physics and Astronomy, University of Edinburgh, United Kingdom
[25] Paul Scherrer Institut (PSI), Villigen, Switzerland
[26] University of Ioannina, Greece
[27] Affiliated with an institute covered by a cooperation agreement with CERN
[28] Goethe University Frankfurt, Germany
[29] Horia Hulubei National Institute of Physics and Nuclear Engineering, Romania
[30] Instituto Superior Técnico, Lisbon, Portugal
[31] European Commission, Joint Research Centre (JRC), Geel, Belgium
[32] Karlsruhe Institute of Technology, Campus North, IKP, 76021 Karlsruhe, Germany
[33] Agenzia nazionale per le nuove tecnologie, l'energia e lo sviluppo economico sostenibile (ENEA), Italy
[34] Istituto Nazionale di Fisica Nucleare, Sezione di Bologna, Italy
[35] Dipartimento di Fisica e Astronomia, Università di Bologna, Italy
[36] INFN Laboratori Nazionali di Legnaro, Italy
[37] Istituto Nazionale di Fisica Nucleare, Sezione di Trieste, Italy
[38] Department of Physics, University of Trieste, Italy
[39] Consiglio Nazionale delle Ricerche, Bari, Italy
[40] Istituto Nazionale di Fisica Nucleare, Sezione di Catania, Italy
[41] Physikalisch-Technische Bundesanstalt (PTB), Bundesallee 100, 38116 Braunschweig, Germany
[42] University of Granada, Spain
[43] University of Vienna, Faculty of Physics, Vienna, Austria
[44] Department of Physics, University of Basel, Switzerland
[45] Centre for Astrophysics Research, University of Hertfordshire, United Kingdom
[46] Bhabha Atomic Research Centre (BARC), India
[47] Helmholtz-Zentrum Dresden-Rossendorf, Germany
[48] Australian National University, Canberra, Australia

ARTICLE INFO

Keywords:
Neutron capture cross section
Neutron total cross section
Resonance analysis

ABSTRACT

Accurate neutron capture cross section data for minor actinides are essential for the safe and efficient management of high level radioactive waste produced during the operation of nuclear reactors. In particular, ^{244}Cm, with a half-life of 18.11 years, dominates neutron emission in spent fuel and also contributes significantly to the decay heat and radiotoxicity. Furthermore, neutron capture on ^{244}Cm opens the pathway for the formation of heavier isotopes such as Bk, Cf, and other Cm isotopes. Sensitivity studies for present and future nuclear reactors have highlighted the need to reduce the uncertainties in the ^{244}Cm capture cross section. Experimental data on the capture cross section of this isotope are scarce due to the challenges associated with its measurements. Prior to the presented measurement and two recent measurements conducted at J-PARC, only one set of data for the ^{244}Cm capture cross section existed, obtained in 1969 during an underground nuclear explosion experiment. The capture cross section of ^{244}Cm has been measured at the n_TOF facility at CERN with three different experimental setups: one at Experimental Area 1 (EAR1) using the Total Absorption Calorimeter and two measurements at Experimental Area 2 (EAR2) with C_6D_6 detectors, employing two different samples. The results from these three measurements were found to be compatible and then combined. In total, 17 resonances of ^{244}Cm were measured at n_TOF below 300 eV. The radiative kernels obtained in this measurement are in good agreement with JENDL-4.0 for the majority of the resonances. Additionally, they are compatible with the recent JENDL-5 library below 50 eV, while at higher energies, the majority of radiative kernels from this evaluation based on the recent measurement by Kawase et al., are not compatible. Additionally, the ^{244}Cm samples also contained ^{240}Pu. Resonances of this isotope were analyzed in the energy range between 20 and 180 eV, and the results were found to be consistent with previous measurements and evaluations, that enhances confidence in the ^{244}Cm results.

1. Introduction

The safe and efficient management of high-level radioactive waste produced during the operation of nuclear reactors requires accurate nuclear data. In particular, inventory calculations of Spent Nuclear Fuel (SNF) and derived quantities such as decay heat, radiotoxicity, neutron dose, and gamma dose depend on the available accuracy of neutron-induced reactions governing the burn-up process. Among the isotopes, ^{244}Cm warrants particular attention due to its significant impact throughout the nuclear fuel cycle. It contributes approximately 10% of the radiotoxicity and decay heat in spent nuclear fuel (SNF) from Light Water Reactors (LWRs) during the first 15 years after reactor discharge. Moreover, from 10 to 100 years, about 90% of the neutron emission from SNF is driven by the spontaneous fission of ^{244}Cm (Rochman et al., 2024). As shown in Fig. 1, it continues to dominate the neutron emission up to 200 years after discharge.

Furthermore, studies performed in the context of Accelerator-Driven Systems (ADS) (García-Herranz et al., 2010) have shown that, following fuel irradiation in an ADS, ^{244}Cm plays an even more prominent role in contributing to radiotoxicity, decay heat, and neutron emission.

To identify which nuclear data uncertainties should be reduced to improve spent nuclear fuel (SNF) inventory calculations, sensitivity analyses have been performed. In particular, target accuracy studies for presente and future nuclear systems, as summarized in Ref. Aliberti et al. (2006), highlight the need to minimize the uncertainty in the ^{244}Cm capture cross section. This study recommends reducing the ^{244}Cm capture uncertainty to 4.1% in the energy range from 4 to 22.6 eV, and to 14.4% in the range from 22.6 to 454 eV. Moreover, achieving more precise knowledge of the ^{244}Cm capture cross section is

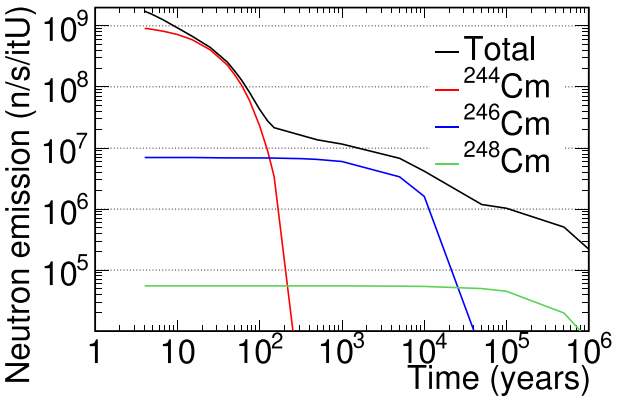

Fig. 1. Calculated neutron emission of the spent fuel per initial ton of uranium (itU) for the main Cm isotopes and for all the elements (Total). The calculations have been done with ORIGEN2 (Croff, 1983) for a Pressurized Water Reactor (PWR) with a 50 GWd/tU burnup after four years in the spent fuel pool.

essential for improving calculations related to the formation of heavier isotopes, including Bk, Cf, and other Cm isotopes.

Only three previous capture measurements of this isotope have been reported. The first was conducted in 1969 using neutrons generated by an underground nuclear explosion, in a single-shot experiment with significant limitations (Moore et al., 1971). The other two measurements were performed at J-PARC using samples from the same batch material employed in the present study. These experiments were carried out by Kimura et al. (2012) and Kawase et al. (2021). The main limitation of both J-PARC measurements was the need of substantial corrections due to pile-up effects.

The capture cross sections of ^{244}Cm presented in this work were measured at the n_TOF Experimental Area One (EAR1) (Guerrero et al., 2013) and Experimental Area Two (EAR2) (Weiss et al., 2015; Sabaté-Gilarte et al., 2017). These experimental campaigns were conducted in 2017 using the Total Absorption Calorimeter (TAC) detector (Guerrero et al., 2009) at EAR1 and three BICRON C_6D_6 detectors (Plag et al., 2003) at EAR2. Two distinct samples, referred to here as sample A and sample B, were employed in the experiments. For the campaign at EAR1, only the sample A was utilized, whereas both samples were used in the EAR2 campaign. Additionally, during the EAR2 campaign, the capture cross sections of ^{246}Cm and ^{248}Cm were obtained using sample B, and these results have already been published in Ref. Alcayne et al. (2024). The high instantaneous flux of EAR2, in combination with the fast C_6D_6 detectors, helps to overcome the main limitations of the measurements by Kimura et al. and Kawase et al. In addition, combining these data with those from EAR1 helps to reduce uncertainties and increases confidence in the presented results.

2. Experimental setup

2.1. n_TOF facility

Neutrons at n_TOF are produced through spallation reactions induced by a 20 GeV/c pulsed proton beam impinging on a lead target. At the time of the experiment, two experimental areas were operational at n_TOF: EAR1 (Guerrero et al., 2013), located approximately 185 m vertically above the spallation target, and EAR2 (Weiss et al., 2015), situated about 20 m horizontally from the target. The neutron flux in EAR2 is approximately 40 times higher than in EAR1 at relevant neutron energies, whereas the energy resolution is better in EAR1.

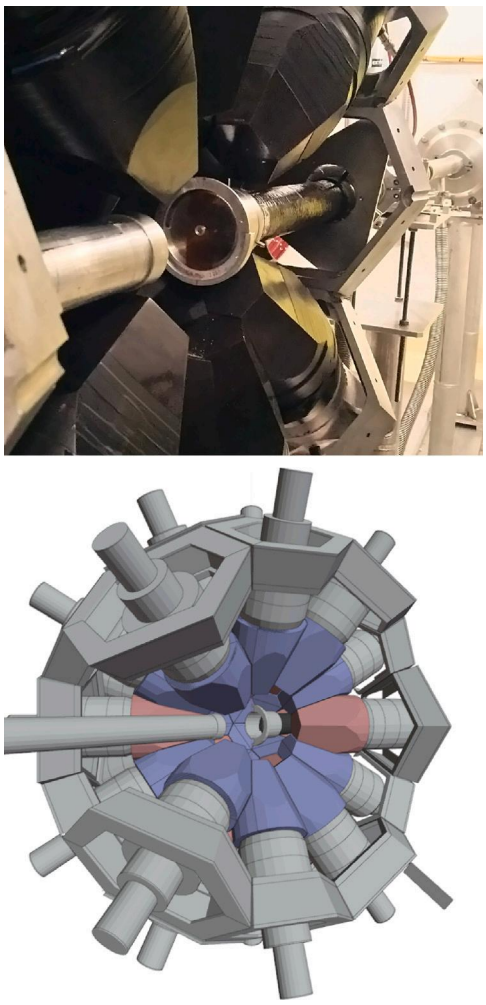

Fig. 2. Top panel: photograph of the TAC detector at EAR1. Only one of the hemispheres is visible in the image. Bottom panel: geometry implemented in Geant4 (Agostinelli et al., 2003) to simulate the detector response, with several crystals removed to reveal the internal structure.

2.2. Detection setups

The proton beam was monitored using a wall current monitor detector, which measures the proton current in each pulse before it impinges on the lead target. Additionally, the neutron beams at EAR1 and EAR2 were monitored using the SiMon (Marrone et al., 2004) and SiMon2 (Cosentino et al., 2015) detectors, respectively. These detectors measure the neutron flux using a configuration of four silicon pad detectors positioned outside the beam, facing a ^{6}LiF foil.

The ^{244}Cm(n, γ) reactions at EAR1 were measured using the TAC (Guerrero et al., 2009), a detector consisting of an array of 40 BaF_2 crystals covering nearly 4π, as shown in Fig. 2. This detector has been employed for over fifteen years to measure capture cross sections of actinides (Guerrero et al., 2012; Mendoza et al., 2014b; Wright et al., 2017; Mendoza et al., 2018; Balibrea-Correa et al., 2020).

The ^{244}Cm(n, γ) reactions at EAR2 were measured using three C_6D_6 detectors (Plag et al., 2003), positioned 5 cm from the center of the sample. A general view of the experimental setup is shown in the top panel of Fig. 3. These detectors have already been employed to measure numerous actinide cross sections in the past (Gunsing et al., 2012; Fraval et al., 2014; Mingrone et al., 2017; Mastromarco et al., 2017; Lerendegui-Marco et al., 2018).

All the signals from the individual detectors have been recorded by the n_TOF Digital Acquisition System (DAQ) (Abbondanno et al., 2005),

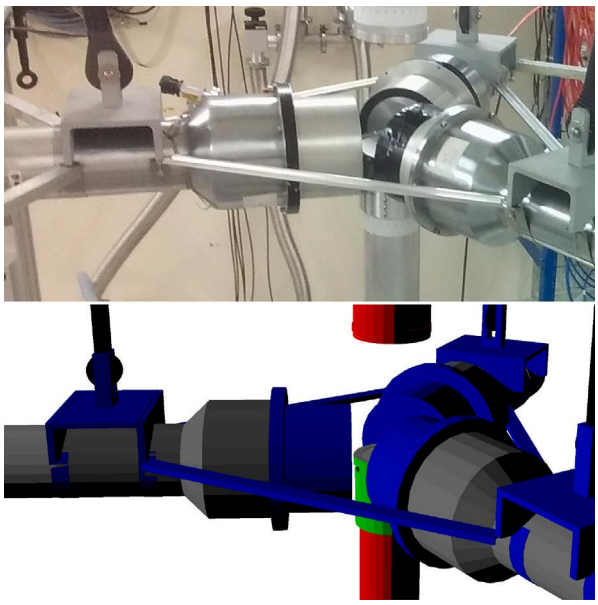

Fig. 3. Top panel: photograph of the experimental setup used in the measurement, consisting of three C_6D_6 detectors at EAR2. Bottom panel: geometry implemented in Geant4 to simulate the detector response.

Table 1
Isotopic abundances (in percent) during the Cm n_TOF measurement campaign for the two samples, in August 2017.

Isotope	Sample A	Sample B
^{240}Pu	30.8 ± 0.6	9.2 ± 0.2
^{243}Am	0.6 ± 0.1	1.2 ± 0.2
^{244}Cm	59.9 ± 1.1	20.1 ± 0.4
^{245}Cm	2.4 ± 0.3	1.0 ± 0.3
^{246}Cm	6.3 ± 0.3	57.0 ± 1.2
^{247}Cm	–	2.8 ± 0.4
^{248}Cm	–	8.7 ± 0.2

based on SPDevices ADQ412DC-3G cards with 1 GSample/s sampling rate and 14 bits resolution.

2.3. Samples

The samples used in the experiment were acquired by the Japan Atomic Energy Agency (JAEA) from the Russian Research Institute of Atomic Research in 2007. The samples consist of Cm oxide pellets with dimensions of 2.5 mm (radius) × 0.5 mm (height), enclosed in an aluminum casing.

Sample A consists of two pellets and contains approximately 0.8 mg of ^{244}Cm, whereas sample B consists of a single pellet with approximately 0.4 mg. The absolute masses of the different isotopes are not precisely known; however, the isotopic mole fractions at the time of the measurement (summer 2017) were determined and are presented in Table 1. These values were derived from the isotopic evolution, taking into account concentrations measured in 2010 (Kimura et al., 2012) and the radioactive decay.

The sample contains several Cm isotopes along with ^{240}Pu, which is produced by the α-decay of ^{244}Cm ($T_{1/2}$ = 18.11 years (Chechev, 2006)).

3. EAR1 data analysis

3.1. Data reduction

The data reduction of the EAR1 measurement in this work follows the procedures used in previous analyses performed with the TAC (Guerrero et al., 2012; Mendoza et al., 2014b; Wright et al., 2017; Mendoza et al., 2018). The digitized BaF_2 (Marrone et al., 2006) signals were analyzed, accounting for fast and slow scintillation components. α-particle signals from the impurities were removed via a fast-to-slow ratio cut, while their amplitude spectra were used to monitor the detector gain, which varied by up to 10% along the experiment.

The signals from all individual detectors were grouped into TAC events using a coincidence window of 20 ns. Each TAC event is characterized by its time-of-flight, total deposited energy (E_{sum}), and the number of BaF_2 crystals contributing to the event (multiplicity, m_{cr}). The reasonable energy resolution, high segmentation, and high detection efficiency of the TAC allow for the identification and rejection of background events through cuts applied to m_{cr} and E_{sum} (Guerrero et al., 2009). In this analysis, the cuts applied were $2.5 > E_{sum}$ (MeV) > 6 and $m_{cr} > 2$. These cuts were selected to improve the signal-to-background ratio without significantly reducing the detection efficiency (Alcayne, 2022). Additionally, an energy threshold of 300 keV was applied to the individual BaF_2 crystals.

The energy calibration and resolution of each crystal were determined using four γ-ray sources (^{137}Cs, ^{88}Y, Am-Be, and Cm-C).

In several previous measurements with the TAC, pile-up corrections were necessary due to counting rates higher than 0.1 counts/μs (Mendoza et al., 2014a; Mendoza, 2014). In this experiment, the small mass of the sample resulted in counting rates below 0.04 counts/μs. Consequently, no pile-up corrections were required.

3.2. Background

The backgrounds in the measurement can be divided into three components:

1. The background not related to the neutron beam is mainly produced by the activity of the Cm sample. This experimentally determined background is low, due to the deposited energy and multiplicity cuts, as illustrated in Fig. 4 (Background 1).
2. The neutron beam dependent background determined using a dummy sample identical to the Cm sample but without any actinide. This background is also presented in Fig. 4 (Background 2).
3. The background produced by the interaction of the neutron beam with the actinides of the sample. The resonances of the different actinides in the sample are sufficiently separated from those of ^{244}Cm, so the reactions in the contaminants of the sample do not represent a significant issue. The background due to nuclear reactions in ^{244}Cm, elastic scattering and fission, has been determined and subtracted from their corresponding detection efficiencies and evaluated cross sections. The detection efficiency for elastic scattering reactions was determined as a function of the neutron energy through a measurement performed with an aluminum sample (Alcayne, 2022). The value for the fission efficiency, 0.37 ± 0.05, has been taken from Ref. Balibrea-Correa et al. (2020).

3.3. (n, γ) detection efficiency

In this experiment, the yield of ^{244}Cm was normalized to that of the first resonance of ^{240}Pu at 1.05 eV. The efficiency for detecting capture reactions (ε_γ) in principle depends on the resonance. However, in the specific cases of radiative neutron capture on ^{244}Cm and ^{240}Pu, both with 0^+ ground states, the resulting compound nuclei have millions of levels below the neutron separation energy. Therefore, the detection efficiencies were assumed to be constant and were determined using Monte Carlo simulations of the capture cascades, following the procedure adopted in previous n_TOF studies on actinides (Guerrero et al., 2012; Mendoza et al., 2014b; Wright et al., 2017; Mendoza et al., 2018). Photon strength functions and level densities used for generating

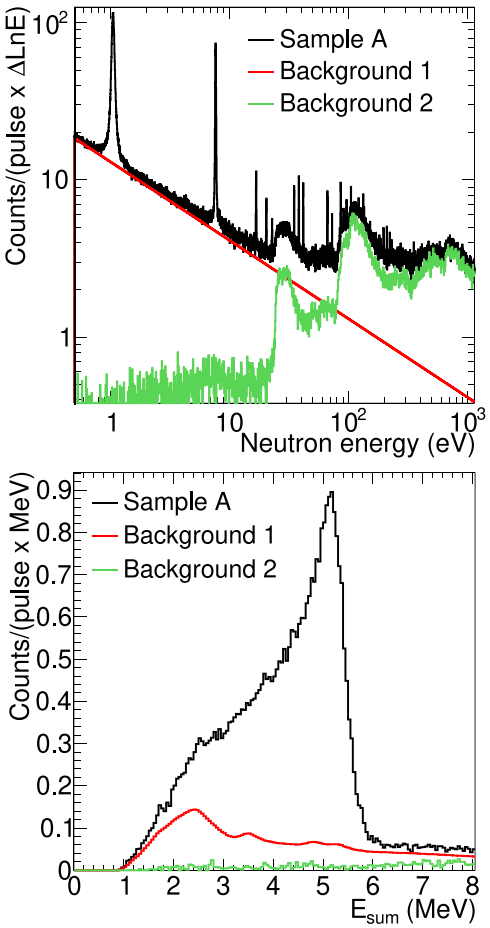

Fig. 4. Measured spectra from the ^{244}Cm sample in EAR1, including the different background components (see text for details). Top: neutron energy spectrum with cuts 2.5 < E_{sum}(MeV) < 6 and m_{cr} > 2. Bottom: E_{sum} for the first ^{244}Cm resonance (7.4 < E_n (eV) < 7.8) with m_{cr} > 2.

Table 2
Neutron capture detection efficiencies (ε_γ) for 2.5 < E_{sum} (MeV) < 6.0 and different m_{cr} cuts.

m_{cr}	$\varepsilon_\gamma(^{240}Pu)$	$\varepsilon_\gamma(^{244}Cm)$	$\varepsilon_\gamma(^{240}Pu)/\varepsilon_\gamma(^{244}Cm)$
0>	0.802(3)	0.805(2)	0.996(4)
1>	0.777(4)	0.778(4)	0.999(7)
2>	0.589(7)	0.589(7)	1.000(17)
3>	0.278(6)	0.282(6)	0.983(28)
4>	0.080(2)	0.083(2)	0.964(39)

^{244}Cm and ^{240}Pu cascades by NuDEX have been adjusted to reproduce the experimental deposited energy spectra, as described in detail in Mendoza et al. (2020). The accurate reproduction of these cascades with experimental results is shown in Fig. 5, and the efficiencies are presented in Table 2.

The uncertainties in Table 2 were estimated by slightly varying the parameters used to generate the cascades. Since the ^{244}Cm yield is normalized to that of ^{240}Pu, the result depends only on the efficiency ratio, which has a 1.7% uncertainty for the cuts of the measurement.

3.4. Capture yield

The capture yield of an isotope i, $Y_{\gamma,i}(E_n)$, is calculated as the fraction of neutrons impinging on the sample that induce a (n, γ) reaction in that isotope. The yield is related to the capture cross section

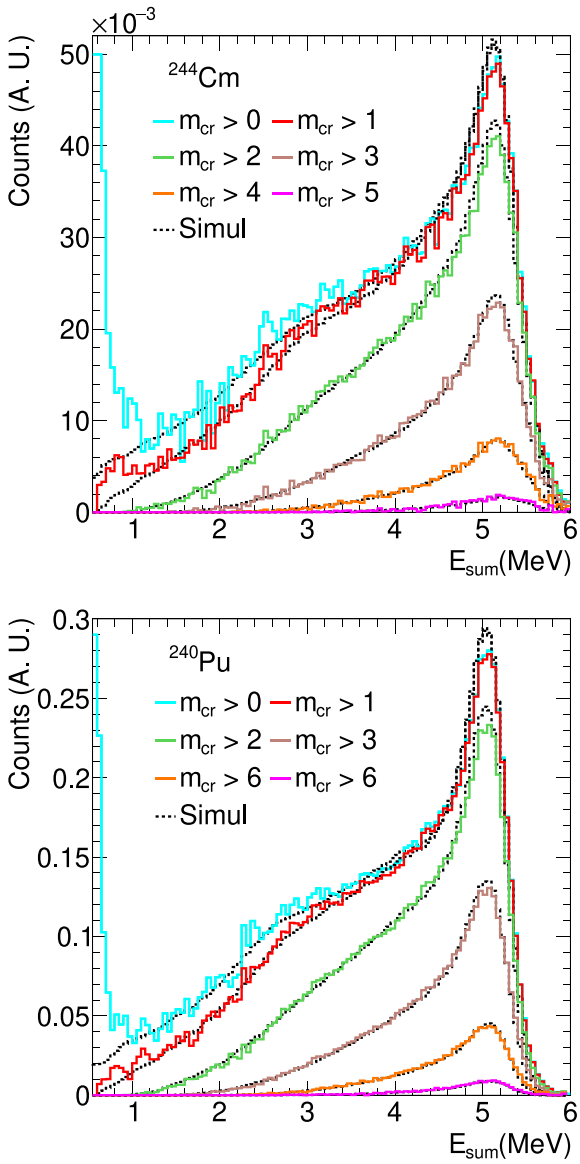

Fig. 5. Comparison between experimental and simulated (Simul) total deposited energy spectra for ^{244}Cm (7.4 < E_n (eV) < 7.8) and ^{240}Pu (0.9 < E_n (eV) < 1.1) capture cascades in the TAC, for different cuts on the detected multiplicity m_{cr}.

of the isotope ($\sigma_{\gamma,i}$) with:

$$Y_{\gamma,i}(E_n) = F_{ms}(E_n)(1 - e^{-n\cdot\sigma_{tot}(E_n)}) \cdot \frac{A_i \cdot \sigma_{\gamma i}(E_n)}{\sigma_{tot}(E_n)} \quad (1)$$

where n is the number of atoms per sample unit area, A_i is the atom fraction of that isotope, σ_{tot} is the sum of the total cross sections of all the isotopes present in the sample, weighted by their isotopic abundances, and F_{ms} is a factor to correct for the multiple interaction effects. This theoretical yield can then be compared with the experimental one to obtain the capture cross section of the isotope. The experimental yield can be determined as follows:

$$Y_{\gamma,exp} = \frac{C - B}{\varepsilon_\gamma \cdot \phi_n} \quad (2)$$

where C is the total sample counting rate, B is the background counting rate, ε_γ is the capture detection efficiency, and ϕ_n is the neutron flux, i.e., the number of neutrons impinging on the sample per unit time.

The time-of-flight to energy conversion was performed using a time-of-flight distance of 185.6(1) m. This value was determined by adjusting the measured ^{197}Au(n, γ) yield with JEFF-3.3 (Plompen et al., 2017). The neutron flux (ϕ_n) was calculated by multiplying the total flux of a sample covering all the beam by the Beam Interception Factor (BIF), which represents the fraction of neutrons intercepted by the sample. The total flux was measured with the SiMon neutron detector (Marrone et al., 2004) that completely covers the beam. The BIF of the Cm sample was determined using the saturated resonance method (Macklin et al., 1979; Borella et al., 2007) at the first resonance of ^{197}Au at 4.9 eV. For this purpose, a gold sample with the same radius as the Cm pellet has been measured obtaining a BIF of 6.10(9)% of the total flux.

3.5. Uncertainties

Concerning the uncertainties, in addition to those due to counting statistics, the following contributions have been considered:

1. Uncertainty in the normalization. The ^{244}Cm yield is normalized with respect to the first resonance of ^{240}Pu, and the associated uncertainties are as follows:
   - Uncertainty in the efficiency ratio $\varepsilon_{\gamma^{240}Pu}/\varepsilon_{\gamma^{244}Cm}$, estimated to be 1.7% (Section 3.3).
   - Uncertainty in the calculation of the ratio between the ^{240}Pu and ^{244}Cm masses, estimated to be 2.8% (Table 1).

   The total uncertainty in the normalization was calculated by adding these two uncertainties, resulting in 3.3%. Additionally, the 2.75% uncertainty in the capture cross section of ^{240}Pu in JEFF-3.3 (Plompen et al., 2017) for the first resonance at ~1 eV was taken into account.
2. Uncertainty in the energy dependence of the neutron flux, estimated to be 1% (Barbagallo et al., 2013).
3. Uncertainty in the neutron beam background subtraction. The systematic uncertainty in the determination of the background was estimated to be 1%, considering the precise background determination with the Dummy sample.
4. Uncertainty in the subtraction of the background related to fission and elastic scattering reactions. They were estimated based on the uncertainties in the detection efficiencies and the evaluated cross sections (Alcayne, 2022).

4. EAR2 data analysis

The analysis procedure for samples A and B at EAR2 follows the same methodology outlined in Alcayne et al. (2024). The main steps of the procedure are summarized in the following list:

- The energy calibration and resolution of each C_6D_6 detector were determined by comparing the detector responses obtained experimentally with those simulated using Monte Carlo methods for various calibration γ-ray sources (Alcayne et al., 2024).
- The same background components presented for the EAR1 yield in Section 3.2 have been considered and subtracted:
  1. The background not related to the neutron beam is caused by the activity of the samples and is shown in Fig. 6 (Background 1).
  2. Neutron beam dependent background. This component was calculated using a dummy sample following the process explained in Ref. Alcayne et al. (2024) and is also presented in Fig. 6 (Background 2).

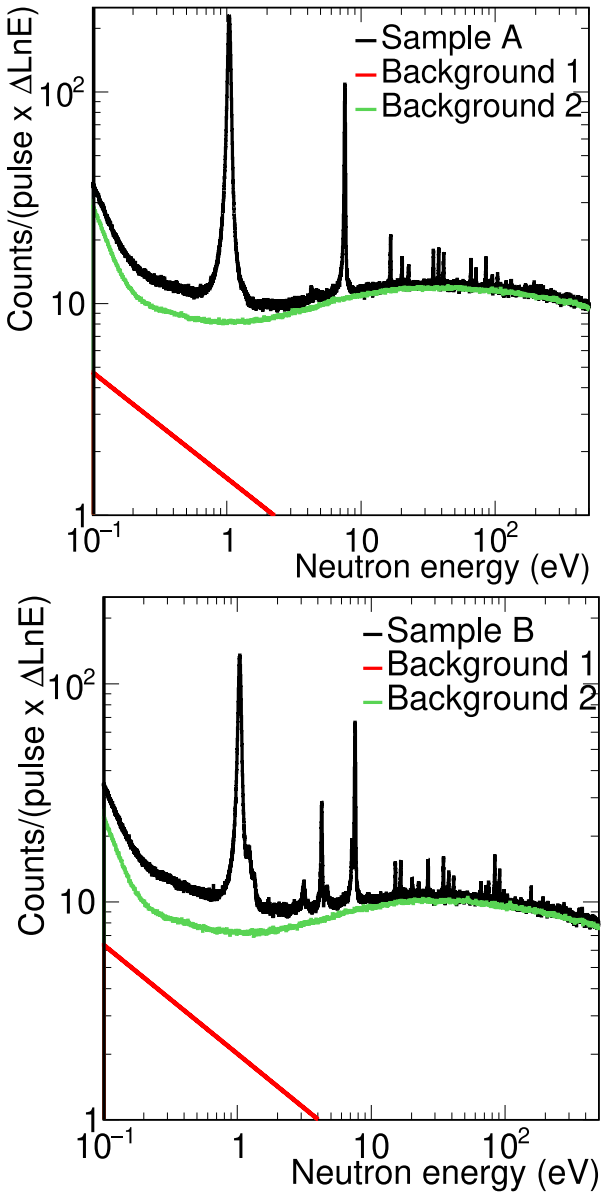

Fig. 6. Counting rate for samples A (top) and B (bottom) with 0.12 < E_{dep} (MeV) < 6 at EAR2 including the different background components (see text for details).

  3. Background produced by the fission reactions in the actinides of the sample. This background has been determined with the fission cross sections of the actinides and the efficiency to detect a fission event (ε_{fis} = 0.085(22)) (Alcayne et al., 2024; Alcayne, 2022). The elastic scattering background has been neglected due to the low neutron detection efficiency of the BICRON detectors (Plag et al., 2003).

- Similarly to EAR1, the neutron capture yield has been calculated using Eq. (2) independently for both samples. The counting rates have been calculated with deposited energy cuts of 0.12 < E_{dep} (MeV) < 6.
  As in EAR1, the detection efficiency was approximated as constant, with a deviation smaller than 1% (Mendoza et al., 2023). The efficiencies were determined using the Pulse Height Weighting Technique (PHWT) (Macklin and Gibbons, 1967; Abbondanno et al., 2004; Mendoza et al., 2023). They were obtained by

Table 3
Estimation of the normalization uncertainties.

Uncertainty (%)	Sample A	Sample B
Abundance ^{240}Pu/^{244}Cm	2.8	2.5
$\varepsilon_{\gamma,^{240}\mathrm{Pu}}/\varepsilon_{\gamma,^{244}\mathrm{Cm}}$	0.5	0.5
Total quadratic sum	2.9	2.7

normalizing the experimental yields measured in this work to those derived using the PHWT.

- The uncertainties in the yield due to systematic effects were determined. They include:

1. The uncertainties associated with the normalization are presented in Table 3. In addition to these uncertainties, the 2.75% uncertainty in the capture cross section of ^{240}Pu in JEFF-3.3 was taken into account.
2. Uncertainty in the gain shifts correction of the energy calibration (Alcayne et al., 2024).
3. Uncertainty in the energy dependence of the neutron flux, estimated to be 1% (Sabaté-Gilarte et al., 2017).
4. Uncertainty in the beam related background subtraction. The uncertainty due to systematic effects, estimated to be 0.4% for both samples (Alcayne et al., 2024).
5. Uncertainty in the fission background produced by the actinides in the sample. These uncertainties were estimated based on the uncertainties in the detection efficiency and the evaluated cross sections (Alcayne, 2022).

5. Resonances analysis

5.1. Methodology

The three capture yields were analyzed independently using the SAMMY code (Larsson, 2006) to determine the Resonance Parameters (RPs) within the framework of R-matrix theory (Frohner, 2000). The detailed methodology is described in Alcayne et al. (2024), Alcayne (2022), and only a brief summary is presented here. Several experimental effects were accounted for in the fitting process, including multiple interaction effects, Doppler broadening corrections using the Free Gas Model (FGM), and resolution broadening, described by the resolution function (RF). For EAR1, a common RF is employed for most experiments (Lorusso et al., 2004). In contrast, EAR2 require an experiment-specific RF adjustment (Vlachoudis et al., 2021) due to its dependence on the sample size. Additionally, fission and elastic scattering background contributions were subtracted using a recursive method (Alcayne et al., 2024).

In this experiment, we are primarily sensitive to the resonance areas rather than their shapes. For this reason, with the exception of the 7.6 eV resonance we varied only the resonance energy (E_0) and the neutron width (Γ_n) in the fitting procedure. For several resonances, namely those with $\Gamma_n \ll \Gamma_\gamma$, the neutron width is the parameter that most strongly correlates with the resonance area. Although Γ_γ affects the resonance area once it becomes comparable to or smaller than Γ_n, this width is expected to be approximately constant within a few percent in actinides (Mughabghab, 2018). We thus fixed Γ_γ to 39.0 meV, as derived from the 7.6 eV resonance (Section 5.3). The Γ_f were taken from JENDL-4.0 (Shibatai et al., 2011). All the resonances are clearly of s-wave origin, with $J = 1/2$. The E_0 and Γ_n were determined independently from the three measured capture yields. These yields, together with the corresponding fits, are shown in Figs. A.11, A.12, and A.13.

5.2. Normalization to ^{240}Pu

As previously mentioned the capture yields of ^{244}Cm have been normalized to the first resonance of ^{240}Pu using the cross section provided by JEFF-3.3 (Plompen et al., 2017). The uncertainties in the normalization for the different samples and experimental areas are approximately 3%, as reported in Sections 3.5 and 4. The main contributor to this uncertainty is the isotopic abundance.

For the normalization, only the ^{244}Cm/^{240}Pu ratio is required. However, determining the absolute masses of the individual isotopes is essential for correcting multiple interaction and self-shielding effects. For sample A, the deduced masses of ^{240}Pu are 0.310(6) mg and 0.312(7) mg for the EAR1 and EAR2 measurements, respectively (Alcayne, 2022). The agreement between these values, obtained using different detectors and experimental conditions, demonstrates consistency in the analysis and reinforces confidence in the normalization. For sample B, the obtained mass is 0.159(4) mg.

5.3. Resonance parameters obtained at EAR1

The Γ_n and E_0 parameters for a total of seven resonances have been fitted from the EAR1 yield in the energy range below 100 eV, as presented in Table A.6. The uncertainties in the yield, as described in Section 3.5, have been propagated to the parameters (Alcayne et al., 2024). For the first two resonances, the dominant source of uncertainty in the Γ_n arises from the normalization, whereas for the remaining resonances, it is primarily due to counting statistics.

Additionally, the radiative width (Γ_γ) of the first resonance at 7.6 eV has been determined. The observed resonance width is not yet dominated by the resolution function (RF), and therefore remains sufficiently sensitive to the natural width, which is governed by Γ_γ. For all remaining resonances, the uncertainties in Γ_γ exceed 50%; consequently, this parameter was not fitted. The Γ_γ value obtained for the 7.6 eV resonance at EAR1 is presented in Table 5.3, alongside previous measurements (Alcayne, 2022). The result from this work is only compatible with two of the four previous measurements.

Measurement	Radiative width (meV)
Coté et al. (1964)	37.5 ± 2.1
Berreth et al. (1972)	35.0 ± 2.0
Kimura et al. (2012)	38.1 ± 2.9
Kawase et al. (2021)	36.1 ± 0.5
This work	39.0 ± 1.5

5.4. Resonance parameters obtained at EAR2

A total of 17 and 9 resonances of ^{244}Cm were fitted in the capture yields of samples A and B at EAR2, respectively. The fitted values of E_0 and Γ_n, along with their associated uncertainties, are presented in Tables A.7 and A.8. The dominant sources of uncertainty below 100 eV are related to the subtraction of the fission background and the RF signal, while at higher energies, they arise mainly from counting statistics and the subtraction of beam-related background. Fig. A.12 shows the capture yield up to 400 eV; however, due to the considerable uncertainties, the resonances above 300 eV could not be reliably fitted.

5.5. Combination of the resonance parameters

The three aforementioned sets of RPs of ^{244}Cm were combined to derive the final values. To achieve this, correlations and uncertainties across the measurements were considered. For example, uncertainties in the RF are correlated between the two measurements performed at EAR2 with different samples. Similarly, there are correlations between measurements taken in the two experimental areas using the same sample, such as uncertainties in the isotopic abundance of ^{244}Cm

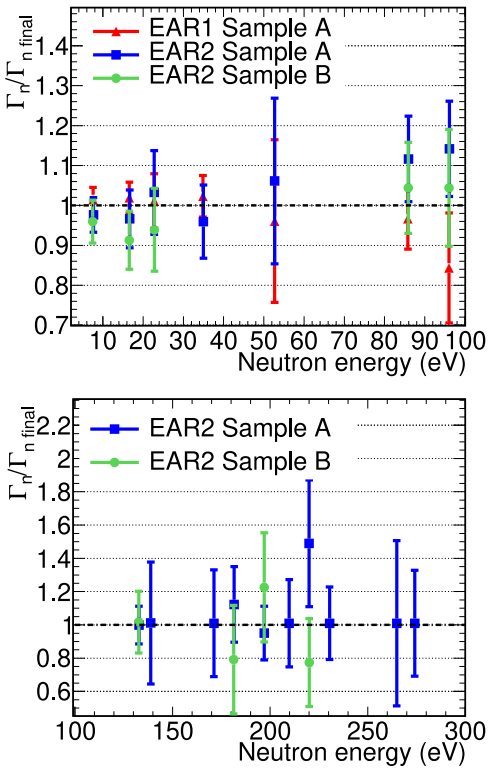

Fig. 7. Ratio between the Γ_n obtained in the three measurements of ^{244}Cm (Tables A.6, A.7, and A.8), and the final value obtained by combining these measurements (Table A.9). The uncertainties consider all the sources of uncertainties except the uncertainty of the nuclear data of ^{240}Pu (2.75%). The uncertainties in $\Gamma_{n\ final}$ has not been considered either.

in the sample. Additionally, within a single measurement, the resonance parameters of different resonances are correlated due to shared uncertainties, such as those related to normalization.

The complexity of this problem, combined with the large number of resonances and associated uncertainties, renders a direct analytical solution without approximations impractical and inefficient. To simplify the calculations, the uncertainties from individual sources were considered as either correlated or uncorrelated, allowing the use of weighted averages to determine the final RPs. A detailed explanation of these calculations is provided in Alcayne (2022).

The final RPs, derived by combining the three measurements, are presented in Table A.9. Additionally, Fig. 7 compares the Γ_n parameters from the three measurements with the combined results. As shown in the figure, the results from all three measurements are compatible.

5.6. Results obtained for ^{240}Pu

As shown in Table 1, a significant amount of ^{240}Pu is present in both samples. Consequently, the resonances of ^{240}Pu have been analyzed using the same procedure applied to ^{244}Cm, also normalizing to the first resonance of ^{240}Pu at 1.06 eV. The RPs obtained from the analysis of the three measurements were again found to be compatible and were combined to produce the final RPs listed in Table A.10.

Additionally, Fig. 8 compares the radiative kernels ($R_k = g_J \Gamma_\gamma \Gamma_n / \Gamma$) for ^{240}Pu, which are proportional to the resonance areas, obtained in this work with those from previous measurements (Coté et al., 1964; Kolar and Böckhoff, 1968; Hockenbury et al., 1969; Kimura et al., 2012; Kawase et al., 2021). As illustrated in the figure, the R_k obtained in this study are consistent with earlier results of ^{240}Pu, thereby reinforcing the reliability of the ^{244}Cm analysis.

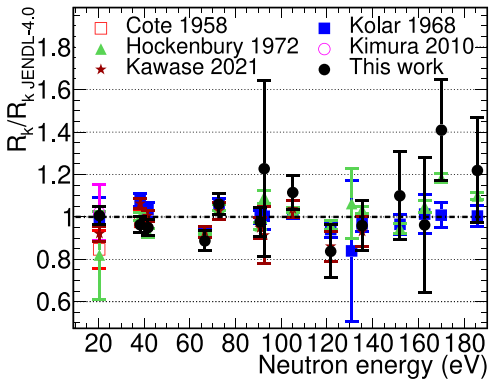

Fig. 8. Ratio between the ^{240}Pu R_k obtained in different experiments in the range from 20 to 190 eV, including this work, and JENDL-4.0.

Table 4
Neutron strength function (S_0) and average level spacing (D_0) for ^{244}Cm s-wave resonances in this work and in previous ones.

	$S_0 \times 10^4$	D_0 (eV)
RIPL-3 (Capote et al., 2009)	1.00(20)	11.8(12)
Mughabghab (Mughabghab, 2018)	0.95(18)	12.1(9)
JENDL-5 (Iwamoto et al., 2023)	1.01	12
This work	0.93(32)	12.1(22)

5.7. Statistical analysis of the resonance parameters

Average resonance parameters of s-wave resonances specifically, neutron strength function, S_0, and the average resonance spacing, D_0 have been obtained from the resonance parameters of ^{244}Cm in Table A.9.

The neutron strength function for s-wave resonances was obtained as $S_0 = \sum_\lambda g\Gamma^0_{n,\lambda}/\Delta E$ (Porter and Thomas, 1956), where ΔE is the width of the energy interval (0–275 eV). The obtained value is $S_0 \times 10^4 = 0.93 \pm 0.32$, considering the uncertainties due to the number of resonances (N) with the formula $\Delta S_0/S_0 = \sqrt{2/N}$ and the uncertainty in experimental determination of $\Gamma^0_{n,\lambda}$.

The average s-wave level spacing can be determined as $D_0 = \Delta E/(N-1)$. However, small resonances often go undetected, and their contribution must be accounted for. Several methods exist to estimate this correction; we employed two approaches. First, the Porter-Thomas distribution can be transformed to determine the number of resonances with $\sqrt{g\Gamma^0_n}$ greater than a certain value, x, can be obtained from:

$$f(x) = \left(\frac{\Delta E}{D_0} + 1\right) \frac{2}{\sqrt{\pi \cdot 2S_0 D_0}} \int_x^\infty \exp\left(-\frac{y^2}{2S_0 D_0}\right) dy. \quad (3)$$

By fitting this formula, the number of missing resonances has been calculated. Considering this missing resonances, the obtained value for D_0 is 12.5 ± 2.4 eV. Second, using Monte Carlo approach we generated several hundreds of artificial resonance sequences from the values of S_0 and Γ_γ obtained in this work and checked the number of missing resonances, similarly to the Refs. Mastromarco et al. (2019) and Lerendegui-Marco et al. (2018). From this approach D_0 = 12.1± 2.2 eV. The results from the two approaches are in agreement

In Table 4, the S_0 and D_0 for ^{244}Cm obtained in this work are compared with various compilations. The evaluations, JEFF-3.3 (Plompen et al., 2017) and ENDF/B-VIII.0 (Brown et al., 2018), provide identical average parameters to those of JENDL-5 (Iwamoto et al., 2023). Overall, the results of this measurement are in agreement with previous compilations and evaluations.

6. Comparison with previous works

Four capture or transmission measurements of ^{244}Cm were conducted prior to 1975, comprising three transmission measurements and

Table 5
Summary of transmission and capture measurements for ^{244}Cm available in the EXFOR database, including the energy ranges in which resonance parameters (RPs) were reported.

Experiment	Type	Energy range
Coté et al. (1964)	Transmission	7–280 eV
Moore et al. (1971)	Capture	22–1000 eV
Berreth et al. (1972)	Transmission	7–100 eV
Belanova et al. (1975)	Transmission	7–180 eV
Kimura et al. (2012)	Capture	7–23 eV
Kawase et al. (2021)	Capture	7–420 eV

one capture measurement, as summarized in Table 5. In addition, two recent capture measurements were performed by Kimura et al. (2012) and Kawase et al. (2021) at J-PARC (Kin et al., 2009).

Regarding the evaluations, the JENDL-4.0 library (Shibatai et al., 2011) is based on the work of Nakagawa (1990), which relies on the older measurements conducted before 1975. The JEFF-3.3 and ENDF/B-VIII.0 libraries have also adopted the JENDL-4.0 values. Furthermore, the recent JENDL-5 evaluation directly incorporates the resonance parameters of Kawase et al. below 420 eV.

In Fig. 9, the R_k obtained in this work are compared with previous measurements and the JENDL-4.0 evaluation. Three resonances reported in JENDL-4.0 at 68, 235, and 242 eV are too small to be observed within the uncertainties of this work; consequently, no information is provided for them. Conversely, the resonances at 139, 171, and 182 eV observed in this measurement and reported in JENDL-4 are not present in the data reported by Kawase. The existence of all these resonances and their assignment to ^{244}Cm are well established, as they appear in samples with different isotopic compositions of Cm and in measurements performed in different experimental areas. However, the uncertainties in R_k vary considerably between resonances; mainly due to counting statistics. The R_k obtained for the majority of resonances are consistent with JENDL-4.0 within one standard deviation. However, 7 resonances are compatible only within two standard deviations and the resonance at 209.8 eV within three standard deviations. At energies below 25 eV, the R_k from the most recent measurement by Kawase are in agreement with those obtained in this work, therefore our data are in agreement with JENDL-5 in this energy range. However, at higher energies, the majority of R_k reported by Kawase are not consistent with our measurements. On average, the R_k of Kawase are 30% lower than those reported in this work and 25% lower than the values in JENDL-4.0.

The uncertainties obtained at n_TOF, as shown in Fig. 10, are often comparable to the lowest values reported in previous measurements by Moore, Coté, and Kawase. However, the results are mutually inconsistent, suggesting either underestimated uncertainties or incorrect determination of the resonance parameters (RPs). The n_TOF data combine the three compatible experiments, reinforcing the reliability of the results.

As mentioned above, the uncertainties for the capture cross section of ^{244}Cm required by Aliberti et al. (2006) for present and future nuclear reactions is at most 4.1% for 4–22.6 eV range. Our data meet this criterion for the radiative kernels of the two resonances within this range. In the energy range between 22.6 and 454 eV, the required uncertainty is then 14.4%. In this range, we determine resonance parameters of a total of 15 resonances below 300 eV, with the uncertainties in R_k of 9 of them falling below this threshold. The resonances with higher uncertainties correspond to smaller resonances, which have a reduced impact on the behavior of nuclear reactors. In conclusion, the new n_TOF measurements, in combination with recent complementary data, provide the foundation for nuclear evaluations that can meet the nuclear data requirements for this isotope.

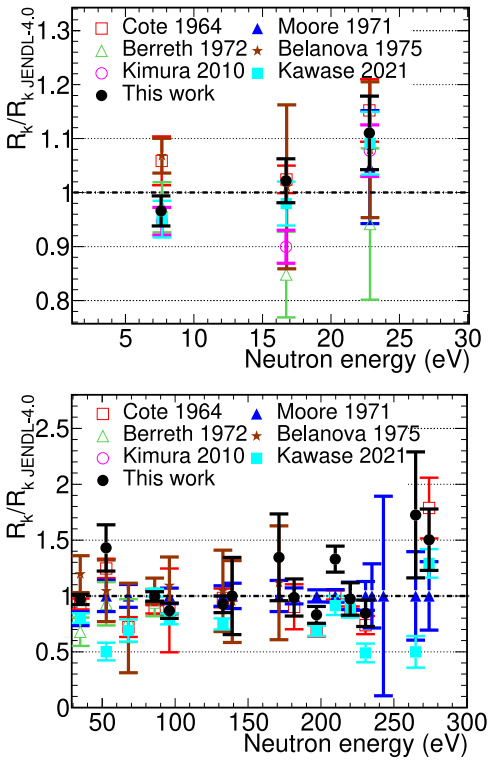

Fig. 9. Ratio between the ^{244}Cm R_k obtained in different experiments in the range from 5 to 300 eV, including this work, and JENDL-4.0.

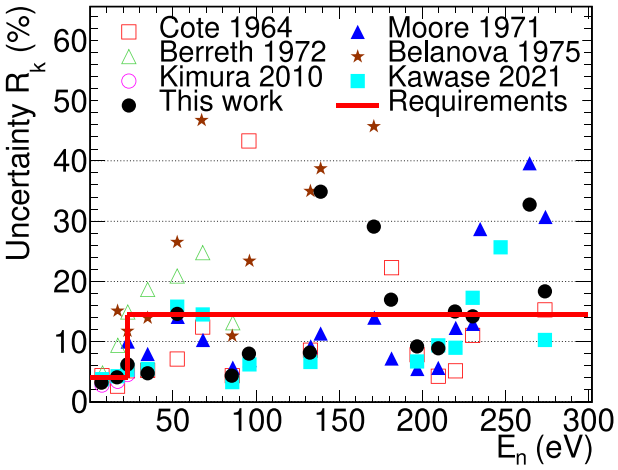

Fig. 10. Comparison between uncertainties in R_k for ^{244}Cm resonances below 300 eV from various works. The requirements for the capture cross section of ^{244}Cm obtained in the sensitivity studies performed by Aliberti et al. are also presented.

7. Summary and conclusions

The capture cross sections of ^{244}Cm have been measured using the time-of-flight technique at the n_TOF facility. The resonance parameters were obtained by combining results from three compatible measurements performed with two different samples in two distinct experimental areas. The measurement in EAR1 was conducted with the TAC detector, while those in EAR2 used C_6D_6 detectors. This is the first time that a capture measurement has been performed in both areas of the n_TOF facility. The high instantaneous fluxes at n_TOF, low pile-up corrections, and the combination of EAR1 and EAR2 data

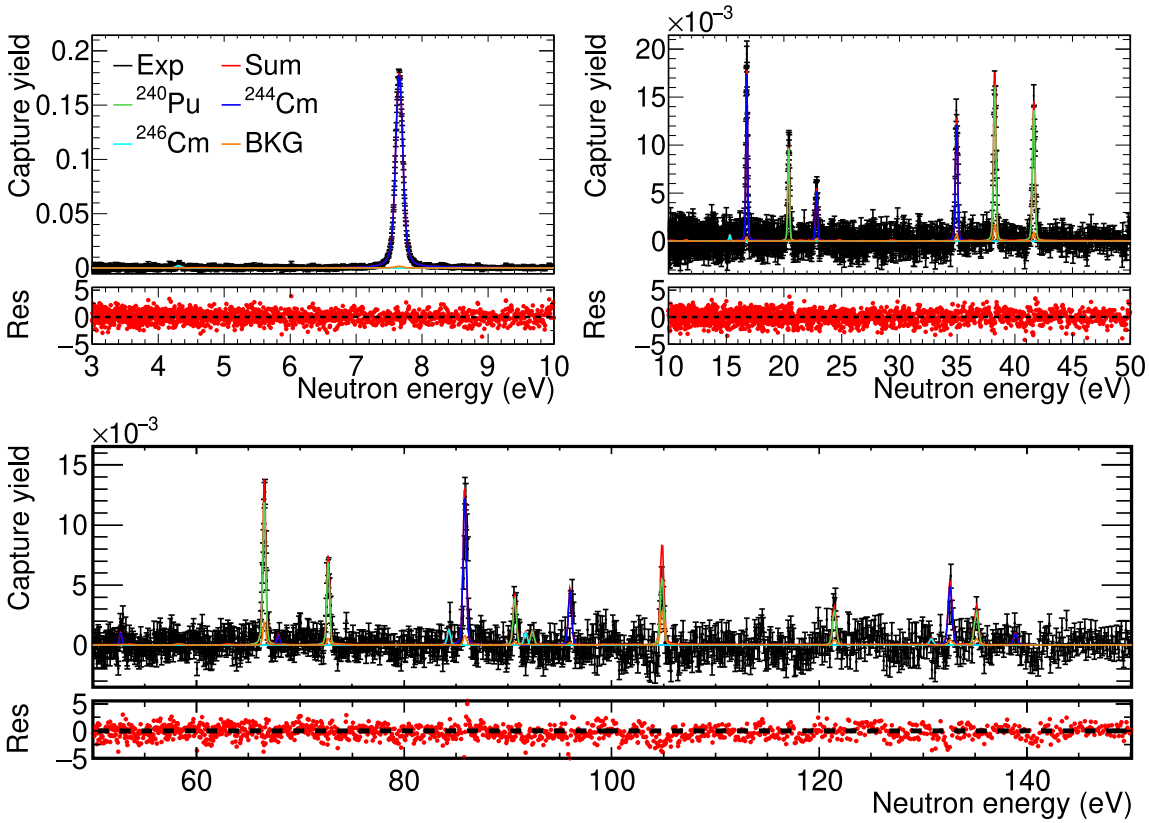

Fig. A.11. Experimental capture yield measured in EAR1 for sample A (Exp), compared with the fitted yields. The experimental capture yield includes only the uncertainties due to counting statistics. The green, blue, and cyan lines correspond to the capture yields for each isotope. The orange line (BKG) represents the background from fission events in the actinides, which has been subtracted in the resonance analysis. The red line (Sum) shows the total yield, including all contributions.

Table A.6
Resonance parameters of ^{244}Cm for sample A obtained in EAR1. The different uncertainties presented in the table are due to: counting statistics (Sta), subtraction of the background produced by the fission events (Fis), subtraction of the beam dependent background (Dummy), subtraction of the background produced by the elastic scattering events (Ela) and normalization (Nor). The uncertainty in the capture cross section of ^{240}Pu (2.75%) has not been included in the table. The different uncertainties are considered to be correlated (CU) or uncorrelated (UU) between the resonances (Alcayne, 2022).

E_0	Γ_n	Γ_n uncertainty (meV)							
		Sta	Fis	Dummy	Ela	Nor	Sum	Sum	Sum
(eV)	(meV)	(UU)	(CU)	(CU)	(UU)	(CU)	(CU)	(UU)	Total
7.664 (3)	9.19	0.04	0.02	0.00	0.03	0.29	0.29	0.06	0.30
16.793 (2)	2.021	0.046	0.014	0.003	0.001	0.065	0.066	0.046	0.081
22.849 (7)	0.939	0.055	0.014	0.005	0.001	0.030	0.033	0.055	0.065
34.999 (5)	4.40	0.17	0.07	0.03	0.01	0.14	0.16	0.17	0.23
52.89 (4)	0.77	0.16	0.01	0.03	0.00	0.02	0.04	0.16	0.16
86.07 (1)	22.7	1.5	0.1	0.4	0.4	0.7	0.8	1.6	1.8
96.32 (3)	5.15	0.78	0.05	0.26	0.03	0.16	0.31	0.78	0.84

obtained with different samples represent the main advantages of this measurement compared with those of Kimura et al. and Kawase et al. Additionally, the ^{244}Cm samples also contained ^{240}Pu. Resonances of this isotope were analyzed in the energy range between 20 and 180 eV, and the results were found to be consistent with previous measurements and evaluations. These results supports the reliability of the ^{244}Cm measurement.

A total of 17 resonances of ^{244}Cm were analyzed below 300 eV. Most of the radiative kernels obtained in this work are consistent with the JENDL-4.0 values. At energies below 25 eV, our results are compatible with the recent work performed by Kawase et al. upon which the new JENDL-5 evaluation is based. However, at energies above 25 eV significant differences were observed, with our radiative kernels being, on average, 30% higher.

The uncertainties achieved at n_TOF are comparable to the lowest previously documented for most resonances. Furthermore, the uncertainty requirements for present and future nuclear reactor applications, as outlined by Aliberti et al. through sensitivity studies, are fulfilled for the majority of the resonances. These new ^{244}Cm results provide valuable experimental input for improving future nuclear data evaluations, contributing to a more accurate description of actinide capture cross sections.

Declaration of competing interest

The authors declare that they have no known competing financial interests or personal relationships that could have appeared to influence the work reported in this paper.

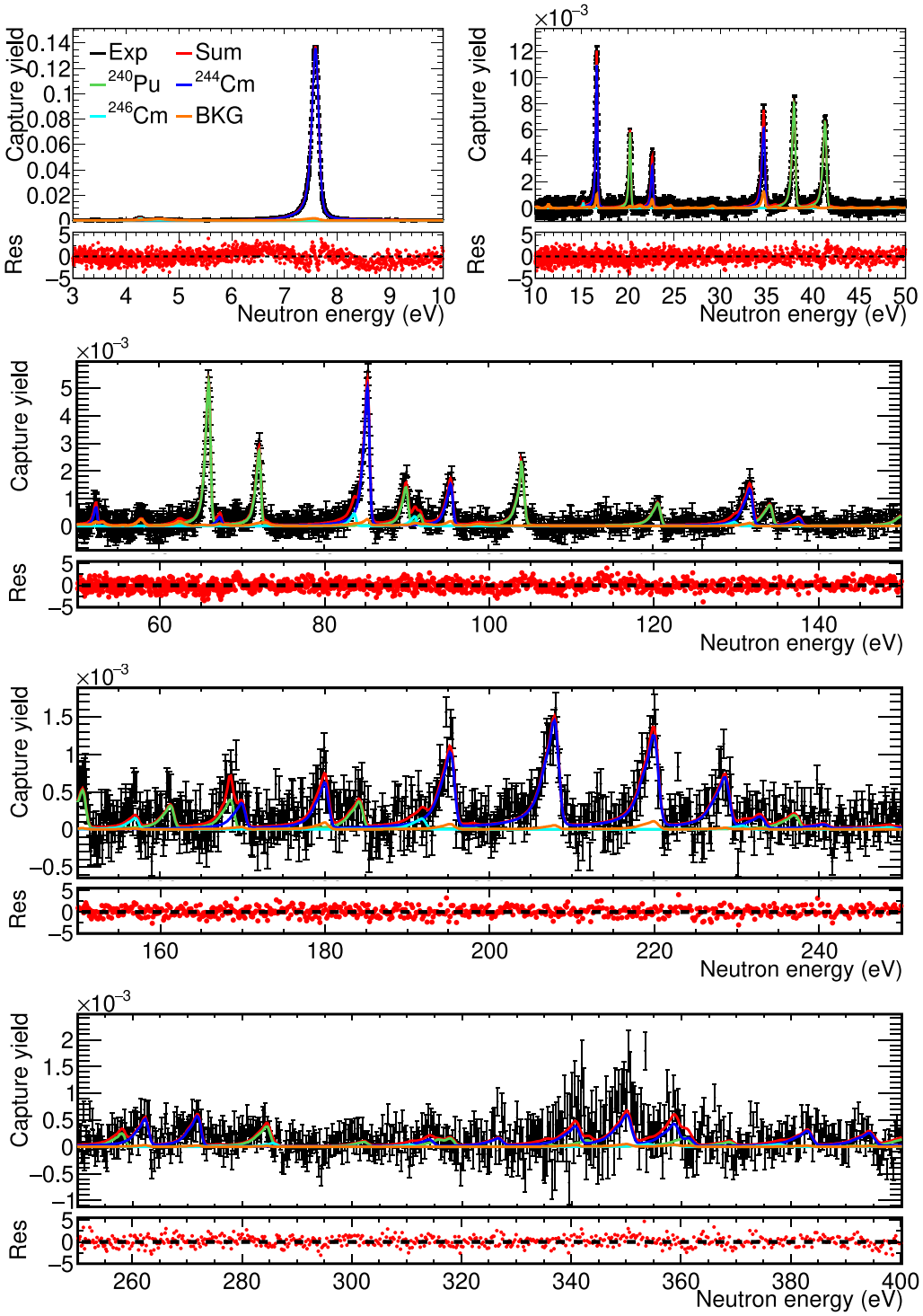

Fig. A.12. Same as Fig. A.11 but for the sample A at EAR2.

Acknowledgments

This work was supported in part by the I+D+i grant PGC2018-096717-B-C21 funded by MCIN/AEI/10.13039/501100011033, by project PID2021-123100NB-I00 funded by MCIN/AEI/10.13039/501100011033/FEDER, UE, by project PCI2022-135037-2 funded by MCIN/AEI/10.13039/501100011033/ and European Union NextGenerationEU/PRTR, by the European Commission H2020 Framework Programme project SANDA (Grant agreement ID: 847552), Croatian Science Foundation project IP-2022-10-3878 and by funding agencies of the n_TOF participating institutions.

Appendix. Resonance fits and parameters

See Figs. A.11–A.13 and Tables A.6–A.10.

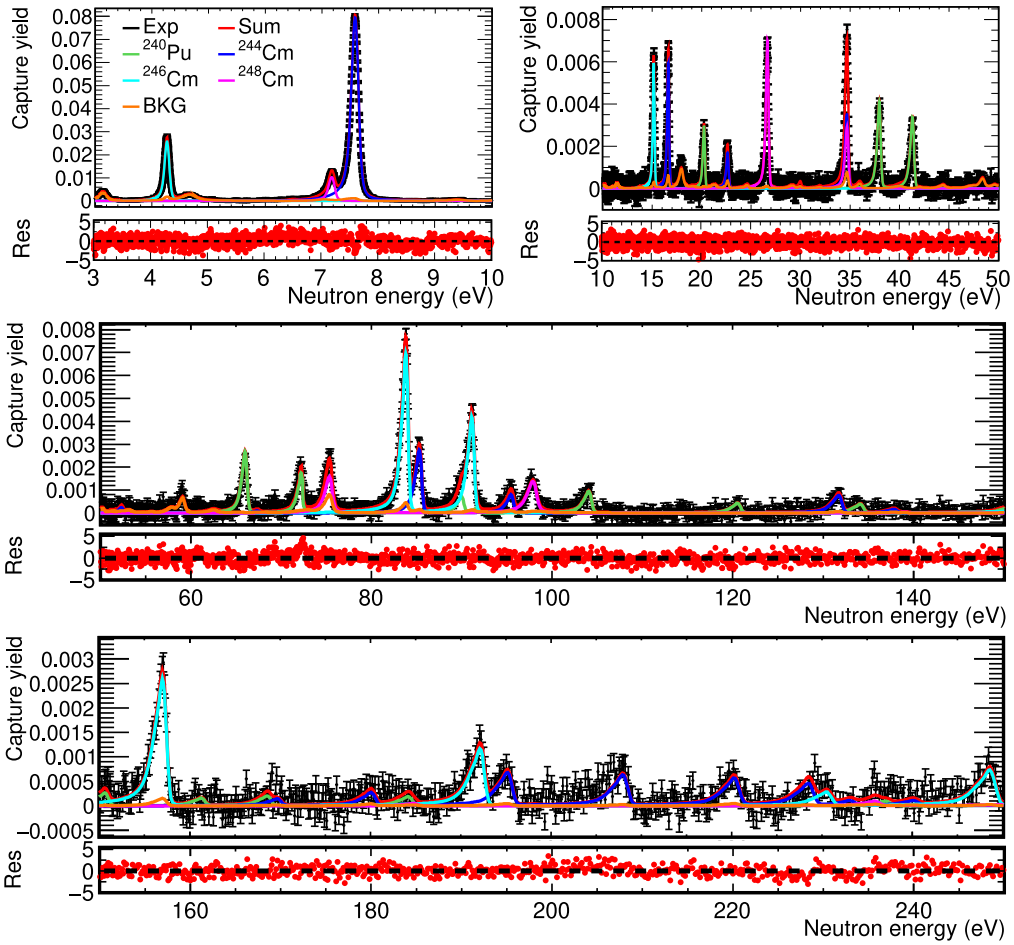

Fig. A.13. Same as Fig. A.11 but for the sample B at EAR2.

Table A.7
Resonance parameters of ^{244}Cm for sample A obtained at EAR2. Some uncertainties are explained in Table A.6. Additional ones correspond to the correction of the gain shifts of the energy calibration (Gain) and the determination of the RF (RF). The uncertainty in the capture cross section of ^{240}Pu (2.75%) has not been included in the table.

E_0	Γ_n	Γ_n uncertainty (meV)								
(eV)	(meV)	Sta (UU)	Fis (CU)	Dummy (CU)	Gain (UU)	RF (UU)	Nor (CU)	Sum (CU)	Sum (UU)	Sum Total
7.664 (3)	8.85	0.01	0.07	0.02	0.03	0.28	0.26	0.27	0.28	0.39
16.792 (2)	1.92	0.01	0.06	0.02	0.01	0.12	0.06	0.08	0.12	0.14
22.835 (4)	0.96	0.02	0.06	0.02	0.00	0.07	0.03	0.07	0.07	0.10
35.002 (2)	4.13	0.06	0.24	0.06	0.03	0.27	0.12	0.28	0.28	0.39
52.81 (2)	0.85	0.09	0.07	0.10	0.03	0.05	0.03	0.13	0.11	0.17
86.06 (1)	26.2	0.7	0.8	0.8	0.1	2.0	0.8	1.4	2.1	2.5
96.25 (2)	7.0	0.4	0.3	0.4	0.1	0.2	0.2	0.6	0.4	0.7
132.89 (3)	13.6	0.9	0.4	1.0	0.1	0.2	0.4	1.2	1.0	1.5
138.9 (2)	2.50	0.61	0.14	0.64	0.14	0.02	0.07	0.66	0.63	0.91
171.4 (2)	4.6	1.0	0.1	1.1	0.0	0.0	0.1	1.1	1.0	1.5
181.6 (1)	10.8	1.5	0.5	1.5	0.2	0.1	0.3	1.6	1.5	2.2
197.0 (1)	27.3	3.0	0.9	3.3	0.2	0.6	0.8	3.5	3.1	4.6
209.8 (1)	79.3	11.5	2.9	14.7	0.7	7.9	2.4	15.2	13.9	20.6
221.9 (1)	70.2	10.6	5.0	11.1	3.7	6.7	2.1	12.4	13.0	17.9
230.6 (2)	22.0	3.4	0.3	3.1	0.5	0.9	0.7	3.2	3.5	4.7
264.6 (3)	20.9	4.1	0.6	9.1	2.0	1.5	0.6	9.1	4.8	10.3
274.2 (3)	29.7	5.8	0.7	6.4	1.9	2.9	0.9	6.5	6.7	9.3

Table A.8
Same as Table A.7 but for sample B.

E_0	Γ_n	Γ_n uncertainty (meV)								
(eV)	(meV)	Sta (UU)	Fis (CU)	Dummy (CU)	Gain (UU)	RF (UU)	Nor (CU)	Sum (CU)	Sum (UU)	Sum Total
7.663 (3)	8.68	0.01	0.08	0.02	0.09	0.39	0.24	0.26	0.41	0.48
16.788 (2)	1.81	0.02	0.06	0.03	0.01	0.11	0.05	0.08	0.12	0.14
22.836 (3)	0.87	0.03	0.05	0.05	0.00	0.05	0.02	0.07	0.06	0.10
86.09 (1)	24.5	1.0	0.7	1.1	0.0	2.0	0.6	1.5	2.2	2.7
96.33 (4)	6.37	0.59	0.30	0.55	0.07	0.14	0.17	0.65	0.61	0.89
132.92 (6)	13.8	1.4	0.5	2.0	0.1	0.1	0.4	2.1	1.4	2.5
181.7 (2)	7.6	1.9	0.4	2.4	0.5	0.2	0.2	2.4	2.0	3.1
196.9 (1)	35.1	6.0	1.4	6.7	1.2	1.9	0.9	6.9	6.4	9.4
222.2 (1)	36.5	7.3	1.8	9.6	2.0	0.8	1.0	9.8	7.6	12.5

Table A.9
Resonance parameter for ^{244}Cm combining the three measurements. The uncertainties in the Γ_n parameter has been separated in two groups the ones that are correlated between the different resonances (Sum CU) and the ones that are uncorrelated (Sum UU). The two uncertainties are added quadratically in the next column. The uncertainty in the capture cross section of ^{240}Pu (2.75%) has not been included in the table.

E_0	Γ_n	Γ_n uncertainty (meV)			R_k
(eV)	(meV)	Sum (UU)	Sum (CU)	Sum Total	(meV)
7.664 (1)	9.06	0.05	0.20	0.20	7.33 (16)
16.792 (2)	1.983	0.043	0.045	0.062	1.825 (57)
22.839 (3)	0.929	0.046	0.025	0.052	0.844 (48)
35.001 (3)	4.30	0.15	0.12	0.19	3.63 (16)
52.84 (3)	0.80	0.11	0.04	0.12	0.75 (11)
86.071 (7)	23.5	1.2	0.7	1.4	14.51 (89)
96.29 (2)	6.10	0.42	0.32	0.53	5.10 (44)
132.90 (4)	13.6	0.8	1.2	1.4	9.9 (10)
138.9 (2)	2.48	0.63	0.65	0.91	2.18 (80)
171.4 (2)	4.5	1.0	1.1	1.5	3.9 (13)
181.6 (1)	9.6	1.2	1.6	2.0	7.4 (15)
196.98 (9)	28.7	2.8	3.4	4.4	16.3 (25)
209.8 (1)	78.5	13.9	15.1	20.5	26.0 (68)
222.0 (1)	47.1	9.2	12.2	15.3	21.0 (68)
230.6 (2)	21.8	3.5	3.2	4.7	13.9 (30)
264.6 (3)	20.7	4.8	9.1	10.3	13.3 (66)
274.2 (3)	29.3	6.7	6.4	9.3	16.6 (53)

Table A.10
Same as Table A.9 but for ^{240}Pu.

E_0	Γ_n	Γ_n uncertainty (meV)			R_k
(eV)	(meV)	Sum (UU)	Sum (CU)	Sum Total	(meV)
20.449 (2)	2.77	0.06	0.10	0.11	2.53 (10)
38.323 (2)	18.3	0.6	1.0	1.2	10.38 (66)
41.718 (3)	16.00	0.46	0.82	0.94	9.83 (58)
66.641 (4)	41.3	2.6	4.0	4.8	18.4 (21)
72.81 (1)	24.3	0.9	1.7	2.0	12.6 (10)
90.80 (2)	12.8	0.7	1.0	1.2	9.05 (85)
92.49 (8)	3.8	1.3	0.7	1.4	3.3 (13)
105.0 (1)	63.2	12.3	7.7	14.5	19.7 (45)
121.6 (1)	11.7	1.7	1.5	2.3	8.6 (17)
135.3 (1)	17.1	2.2	2.1	3.1	11.3 (20)
152.1 (1)	21.5	3.9	3.2	5.1	13.6 (32)
162.6 (2)	8.1	2.6	2.3	3.4	6.3 (27)
170.2 (2)	22.6	3.9	5.4	6.6	13.1 (38)
185.9 (2)	21.7	5.2	5.3	7.4	12.7 (44)

Data availability

Data will be made available on request.

References

Abbondanno, U., et al., The n_TOF Collaboration, 2004. New experimental validation of the pulse height weighting technique for capture cross-section measurements. Nucl. Instrum. Methods A 521, 454–467. http://dx.doi.org/10.1016/j.nima.2003.09.066.

Abbondanno, U., et al., The n_TOF Collaboration, 2005. The data acquisition system of the neutron time-of-flight facility n_TOF at CERN. Nucl. Instrum. Methods A 538, 692–702. http://dx.doi.org/10.1016/j.nima.2004.09.002.

Agostinelli, S., et al., the GEANT4 Collaboration, 2003. Geant4—a simulation toolkit. Nucl. Instrum. Methods A 506 (3), 250–303. http://dx.doi.org/10.1016/S0168-9002(03)01368-8.

Alcayne, V., 2022. Measurement of the Cm-244, Cm-246 and Cm-248 Neutron-Induced Capture Cross Sections at the CERN n TOF Facility (Ph.D. thesis). URL: https://cds.cern.ch/record/2811791?ln=es.

Alcayne, V., et al., The n_TOF Collaboration, 2024. Measurement and analysis of the 246Cm and 248Cm neutron capture cross-sections at the EAR2 of the nTOF facility at CERN. Eur. Phys. J. A 60 (12), 246. http://dx.doi.org/10.1140/epja/s10050-024-01453-w.

Aliberti, G., et al., 2006. Nuclear data sensitivity, uncertainty and target accuracy assessment for future nuclear systems. Ann. Nucl. Energy 33, 700–733. http://dx.doi.org/10.1016/j.anucene.2006.02.003.

Balibrea-Correa, J., et al., n_TOF Collaboration, 2020. Measurement of the α ratio and (n,γ) cross section of ^{235}U from 0.2 to 200 ev at n_TOF. Phys. Rev. C 102, 044615. http://dx.doi.org/10.1103/PhysRevC.102.044615.

Barbagallo, M., et al., 2013. High-accuracy determination of the neutron flux at n_TOF. Eur. Phys. J. A 49 (12), 156. http://dx.doi.org/10.1140/epja/i2013-13156-x.

Belanova, T.S., et al., 1975. Neutron resonances in 244Cm,245Cm,246Cm, and248Cm. Sov. At. Energy 39 (5), 1020–1021. http://dx.doi.org/10.1007/BF01126376.

Berreth, J.R., Simpson, F., Rusche, B.C., 1972. The total neutron cross sections of the curium isotopes from 0.01 to 30 eV. Nucl. Sci. Eng. 49 (2), 145–152. http://dx.doi.org/10.13182/NSE72-A35502.

Borella, A., Aerts, G., Gunsing, F., Moxon, M., Schillebeeckx, P., Wynants, R., 2007. The use of C6D6 detectors for neutron induced capture cross-section measurements in the resonance region. Nucl. Instrum. Methods A 577 (3), 626–640. http://dx.doi.org/10.1016/j.nima.2007.03.034.

Brown, D., et al., 2018. ENDF/B-VIII.0: the 8th major release of the nuclear reaction data library with CIELO-project cross sections, new standards and thermal scattering data. Nucl. Data Sheets 148, 1–142. http://dx.doi.org/10.1016/j.nds.2018.02.001.

Capote, R., et al., 2009. RIPL – reference input parameter library for calculation of nuclear reactions and nuclear data evaluations. Nucl. Data Sheets 110 (12), 3107–3214. http://dx.doi.org/10.1016/j.nds.2009.10.004.

Chechev, V.P., 2006. Evaluation of 242Cm and 244Cm decay data. Phys. At. Nucl. 69 (7), 1188. http://dx.doi.org/10.1134/S1063778806070155.

Cosentino, L., et al., 2015. Silicon detectors for monitoring neutron beams in n-TOF beamlines. Rev. Sci. Instrum. 86, 073509. http://dx.doi.org/10.1063/1.4927073.

Coté, R.E., Barnes, R.F., Diamond, H., 1964. Total neutron cross section of Cm^{244}. Phys. Rev. 134, B1281–B1284. http://dx.doi.org/10.1103/PhysRev.134.B1281.

Croff, A.G., 1983. ORIGEN2: A versatile computer code for calculating the nuclide compositions and characteristics of nuclear materials. Nucl. Technol. 62 (3), 335–352. http://dx.doi.org/10.13182/NT83-1.

Fraval, K., et al., The n_TOF Collaboration, 2014. Measurement and analysis of the 241am(n,gamma) cross section with liquid scintillator detectors using time-of-flight spectroscopy at the n_TOF facility at CERN. Phys. Rev. C 89, 044609. http://dx.doi.org/10.1103/PhysRevC.89.044609.

Frohner, F.H., 2000. Organisation for Economic Co-Operation and Development. Nuclear Energy Agency of the OECD (NEA), Evaluation and analysis of nuclear resonance data.

García-Herranz, N., et al., 2010. Nuclear data requirements for the ADS conceptual design EFIT: Uncertainty and sensitivity study. Ann. Nucl. Energy 37 (11), 1570–1579. http://dx.doi.org/10.1016/j.anucene.2010.06.006.

Guerrero, C., et al., The n_TOF Collaboration, 2009. The n_TOF total absorption calorimeter for neutron capture measurements at CERN. Nucl. Instrum. Methods A 608, 424–433. http://dx.doi.org/10.1016/j.nima.2009.07.025.

Guerrero, C., et al., n_TOF Collaboration, 2012. Measurement and resonance analysis of the ^{237}Np neutron capture cross section. Phys. Rev. C 85, 044616. http://dx.doi.org/10.1103/PhysRevC.85.044616.

Guerrero, C., et al., The n_TOF Collaboration, 2013. Performance of the neutron time-of-flight facility n_TOF at CERN. Eur. Phys. J. A 49, 27. http://dx.doi.org/10.1140/epja/i2013-13027-6.

Gunsing, F., et al., The n_TOF Collaboration, 2012. Measurement of resolved resonances of 232Th(n,gamma) at the n_TOF facility at CERN. Phys. Rev. C 85, 064601. http://dx.doi.org/10.1103/PhysRevC.85.064601.

Hockenbury, R.W., Bartolome, Z.M., Tatarckuz, J.R., Moyer, W.R., Block, R.C., 1969. Neutron radiative capture in Na, Al, Fe, and Ni from 1 to 200 keV. Phys. Rev. 178, 1746–1769. http://dx.doi.org/10.1103/PhysRev.178.1746.

Iwamoto, O., et al., 2023. Japanese evaluated nuclear data library version 5: JENDL-5. J. Nucl. Sci. Technol. 60 (1), 1–60. http://dx.doi.org/10.1080/00223131.2022.2141903.

Kawase, S., et al., 2021. Neutron capture cross sections of curium isotopes measured with ANNRI at J-PARC. J. Nucl. Sci. Technol. 58 (7), 764–786. http://dx.doi.org/10.1080/00223131.2020.1864492.

Kimura, A., et al., 2012. Neutron-capture cross-sections of 244Cm and 246Cm measured with an array of large germanium detectors in the ANNRI at J-PARC/MLF. J. Nucl. Sci. Technol. 49 (7), 708–724. http://dx.doi.org/10.1080/00223131.2012.693887.

Kin, T., et al., 2009. Development of a 4pi germanium spectrometer for nuclear data measurements at J-PARC. In: IEEE Nucl. Sci. Symp. Conf. Rec. . pp. 1194–1197. http://dx.doi.org/10.1109/NSSMIC.2009.5402387.

Kolar, W., Böckhoff, K., 1968. Resonance parameters of 240Pu: Part I—Neutron widths. J. Nucl. Energy 22 (5), 299–315. http://dx.doi.org/10.1016/0022-3107(68)90003-8.

Larsson, N., 2006. Updated User's Guide for SAMMY: Multilevel R-Matrix Fits to Neutron Data Using Bayes Equations. Technical Report, ORNL.

Lerendegui-Marco, J., et al., The n_TOF Collaboration, 2018. Radiative neutron capture on Pu-242 in the resonance region at the CERN n_TOF-EAR1 facility. Phys. Rev. C 97, 024605. http://dx.doi.org/10.1103/PhysRevC.97.024605.

Lorusso, G., et al., The n_TOF Collaboration, 2004. Time–energy relation of the n_TOF neutron beam: energy standards revisited. Nucl. Instrum. Methods A 532 (3), 622–630. http://dx.doi.org/10.1016/j.nima.2004.04.247.

Macklin, R.L., Gibbons, J.H., 1967. Capture-cross-section studies for 30—220-keV neutrons using a new technique. Phys. Rev. C 159 (4), 1007. http://dx.doi.org/10.1103/PhysRev.159.1007.

Macklin, R., Halperin, J., Winters, R., 1979. Absolute neutron capture yield calibration. Nucl. Instrum. Methods 164 (1), 213–214. http://dx.doi.org/10.1016/0029-554X(79)90457-9.

Marrone, S., et al., 2004. A low background neutron flux monitor for the n_TOF facility at CERN. Nucl. Instrum. Methods A 517 (1), 389–398. http://dx.doi.org/10.1016/j.nima.2003.09.060.

Marrone, S., et al., 2006. Pulse shape analysis of signals from BaF2 and CeF3 scintillators for neutron capture experiments. Nucl. Instrum. Methods A 568 (2), 904–911. http://dx.doi.org/10.1016/j.nima.2006.08.064.

Mastromarco, M., et al., The n_TOF Collaboration, 2017. The U-236 neutron capture cross-section measured at the n_TOF CERN facility. EPJ Web Conf. 146, 11054. http://dx.doi.org/10.1051/epjconf/201714611054.

Mastromarco, M., et al., n_TOF Collaboration, 2019. Eur. Phys. J. A 55 (1), 9. http://dx.doi.org/10.1140/epja/i2019-12692-7.

Mendoza, E., 2014. Measurement of the 243Am Capture Cross Section at the n TOF Facility (Ph.D. thesis). URL: https://cds.cern.ch/record/2852035.

Mendoza, E., Cano-Ott, D., Guerrero, C., Berthoumieux, E., 2014a. Pulse pile-up and dead time corrections for digitized signals from a BaF2 calorimeter. Nucl. Instrum. Methods A 768, 55–61. http://dx.doi.org/10.1016/j.nima.2014.09.010.

Mendoza, E., et al., n_TOF Collaboration, 2014b. Measurement and analysis of the ^{243}Am neutron capture cross section at the n_TOF facility at CERN. Phys. Rev. C 90, 034608. http://dx.doi.org/10.1103/PhysRevC.90.034608.

Mendoza, E., et al., n_TOF Collaboration, 2018. Measurement and analysis of the ^{241}Am neutron capture cross section at the n_TOF facility at CERN. Phys. Rev. C 97, 054616. http://dx.doi.org/10.1103/PhysRevC.97.054616.

Mendoza, E., et al., The n_TOF Collaboration, 2020. Study of photon strength functions of 241Pu and 245Cm from neutron capture measurements. EPJ Web Conf. 239, 01015. http://dx.doi.org/10.1051/epjconf/202023901015.

Mendoza, E., et al., 2023. Neutron capture measurements with high efficiency detectors and the pulse height weighting technique. Nucl. Instrum. Methods A 1047, 167894. http://dx.doi.org/10.1016/j.nima.2022.167894.

Mingrone, F., et al., The n_TOF Collaboration, 2017. Neutron capture cross section measurement of U-238 at the CERN n_TOF facility in the energy region from 1 eV to 700 keV. Phys. Rev. C 95, 034604. http://dx.doi.org/10.1103/PhysRevC.95.034604.

Moore, M., et al., 1971. Analysis of the fission and capture cross sections of the curium isotopes. Phys. Rev. C 3, 1656–1667. http://dx.doi.org/10.1103/PhysRevC.3.1656.

Mughabghab, S. (Ed.), 2018. Atlas of Neutron Resonances (Sixth Edition), sixth ed. Elsevier, Amsterdam, http://dx.doi.org/10.1016/B978-0-44-463780-2.00008-6.

Nakagawa, T., 1990. Evaluation of Neutron Nuclear Data for Curium Isotopes. Technical Report, Japan, p. 100, JAERI-M–90-101.

Plag, R., et al., The n_TOF Collaboration, 2003. An optimized C6d6 detector for studies of resonance-dominated (n,gamma) cross-sections. Nucl. Instrum. Methods A 496, 425–436. http://dx.doi.org/10.1016/s0168-9002(02)01749-7.

Plompen, A., et al., 2017. The JEFF-3.3 Nuclear Data Library. Technical Report JEFF Report 22, OECD Nuclear Energy Agency, URL: https://www.oecd-nea.org/dbdata/jeff/.

Porter, C.E., Thomas, R.G., 1956. Fluctuations of nuclear reaction widths. Phys. Rev. 104, 483–491. http://dx.doi.org/10.1103/PhysRev.104.483.

Rochman, D., et al., 2024. EPJ Nucl. Sci. Technol. 10 (9), 83. http://dx.doi.org/10.1051/epjn/2024010.

Sabaté-Gilarte, M., et al., The n_TOF Collaboration, 2017. High-accuracy determination of the neutron flux in the new experimental area n_TOF-EAR2 at CERN. Eur. Phys. J. A 53, 210. http://dx.doi.org/10.1140/epja/i2017-12392-4.

Shibatai, K., et al., 2011. JENDL-4.0: A new library for nucl. Sci. Eng.. J. Nucl. Sci. Technol. 48 (1), 1–30. http://dx.doi.org/10.1080/18811248.2011.9711675.

Vlachoudis, V., et al., 2021. On the Resolution Function of the n_TOF Facility: a Comprehensive Study and User Guide. Technical Report, URL: https://cds.cern.ch/record/2764434.

Weiss, C., et al., The n_TOF Collaboration, 2015. The new vertical neutron beam line at the CERN n_TOF facility design and outlook on the performance. Nucl. Instrum. Methods A 799, 90–98. http://dx.doi.org/10.1016/j.nima.2015.07.027.

Wright, T., et al., The n_TOF Collaboration, 2017. Measurement of the ^{238}U(n,γ) cross section up to 80 keV with the total absorption calorimeter at the CERN n_TOF facility. Phys. Rev. C 96, 064601. http://dx.doi.org/10.1103/PhysRevC.96.064601.